Redox Biology 56 (2022) 102423

Contents lists available at ScienceDirect

Redox Biology

journal homepage: www.elsevier.com/locate/redox

p53 drives necroptosis via downregulation of sulfiredoxin and peroxiredoxin 3

Sergio Rius-Pérez [a], Salvador Pérez [a], Michel B. Toledano [b], Juan Sastre [a,*]

[a] Department of Physiology, Faculty of Pharmacy, University of Valencia, Spain
[b] Oxidative Stress and Cancer Laboratory, Université Paris-Saclay, CEA, CNRS, Institute for Integrative Biology of the Cell (I2BC), Gif sur Yvette, France

ARTICLE INFO

Keywords:
Programmed cell death
Mitochondria
Redox signaling
Acute pancreatitis
Obesity

ABSTRACT

Mitochondrial dysfunction is a key contributor to necroptosis. We have investigated the contribution of p53, sulfiredoxin, and mitochondrial peroxiredoxin 3 to necroptosis in acute pancreatitis. Late during the course of pancreatitis, p53 was localized in mitochondria of pancreatic cells undergoing necroptosis. In mice lacking p53, necroptosis was absent, and levels of PGC-1α, peroxiredoxin 3 and sulfiredoxin were upregulated. During the early stage of pancreatitis, prior to necroptosis, sulfiredoxin was upregulated and localized into mitochondria. In mice lacking sulfiredoxin with pancreatitis, peroxiredoxin 3 was hyperoxidized, p53 localized in mitochondria, and necroptosis occurred faster; which was prevented by Mito-TEMPO. In obese mice, necroptosis occurred in pancreas and adipose tissue. The lack of p53 up-regulated sulfiredoxin and abrogated necroptosis in pancreas and adipose tissue from obese mice. We describe here a positive feedback between mitochondrial H_2O_2 and p53 that downregulates sulfiredoxin and peroxiredoxin 3 leading to necroptosis in inflammation and obesity.

1. Introduction

Necroptosis is a programmed form of cell death morphologically similar to necrosis that is triggered by activation of cell death receptors and formation of the necrosome [1–3]. The necrosome is formed by the interaction between receptor-interacting protein kinase 1 (RIPK1) and receptor-interacting protein kinase 3 (RIPK3) [1,2], which recruits and phosphorylates mixed lineage kinase domain-like (MLKL) [4–6] by the RIPK3 subunit. When phosphorylated, MLKL oligomerizes and becomes competent to form membrane-disrupting pores, which cause the rupture of the plasma membrane and the leakage of intracellular components [7–10]. RIPK1 may determine cell survival or death, and the endogenous molecules released during necroptosis execution can act as damage-associated molecular patterns (DAMPs), which trigger and actively enhance the inflammatory response [5]. Consequently, necroptosis has a crucial role in the pathogenesis of inflammatory diseases and also contributes to multiple disorders, such as heart failure, acute kidney injury, stroke, acetaminophen and ethanol hepatotoxicity, and nonalcoholic steatohepatitis [5,11].

Necrosome-activating pathways linked to mitochondria have emerged as contributors to the necroptosis signaling network [12,13]. In these mitochondrial pathways, necroptosis activation is highly dependent on the generation of mitochondrial reactive oxygen species (mtROS) [14,15], which promote RIPK1 autophosphorylation [16,17]. In addition, in necroptotic cells RIPK3, while decreasing the expression of mitochondrial complexes I and III, increases mitochondrial translocation of NADPH Oxidase 4 (NOX4) to enhance mtROS production [18]. However, the molecular mechanisms of the mitochondrial

List of abbreviations: ATP, adenosine triphosphate; BCA, bicinchoninic acid; BSA, bovine serum albumin; cfDNA, cell free DNA; CHAPS, 3-[(3-Cholamidopropyl) dimethylammonio]-1-propanesulfonate hydrate; CypD, cyclophilin D; DAMPs, damage-associated molecular patterns; DMSO, dimethyl sulfoxide; DTT, dithiothreitol; EDTA, ethylene diaminetetraacetic acid; EGTA, Ethylene glycol-bis(2-aminoethylether)-N,N,N',N'-tetraacetic acid; ELISA, Enzyme-Linked ImmunoSorbent Assay; HMGB1, high mobility group box 1 protein; HRP, horseradish peroxidase; Hsp90, heat shock protein 90; KO, knockout; MLKL, mixed lineage kinase domain-like; mPTP, mitochondrial permeability transition pore; mtROS, mitochondrial reactive oxygen species; NOX4, NADPH Oxidase 4; PBS, phosphate-buffered saline; PFA, paraformaldehyde; PGC1-α, peroxisome proliferator-activated receptor γ co-activator 1 α; PRX1, peroxiredoxin 1; PRX2, peroxiredoxin 2; PRX3, peroxiredoxin 3; RIPK1, receptor interacting protein kinase 1; RIPK3, receptor-interacting protein kinase 3; ROS, reactive oxygen species; RT-qPCR, Quantitative real-time PCR; SRX1, sulfiredoxin; TBP, tata binding protein; TBS-T, Tris Buffered Saline with Tween® 20; TNF-α, tumor necrosis factor alpha; WT, wild-type.

* Corresponding author. Department of Physiology, Faculty of Pharmacy, University of Valencia, Avda. Vicente Andrés Estellés s/n, 40100, Burjasot, Valencia, Spain.

E-mail address: juan.sastre@uv.es (J. Sastre).

https://doi.org/10.1016/j.redox.2022.102423
Received 10 June 2022; Received in revised form 19 July 2022; Accepted 25 July 2022
Available online 20 August 2022

necroptosis pathway are still poorly understood.

Peroxiredoxin 3 (PRX3) is a typical 2-Cys peroxiredoxin family member exclusively localized to the mitochondrial matrix, and the major H_2O_2-degrading enzyme in this organelle [19,20]. In the 2-Cys PRXs catalytic cycle, the peroxidatic cysteine reacts with H_2O_2 to form a sulfenic acid (Cys–SOH) intermediate, with release of H_2O. The peroxidatic cysteine sulfenate then condenses with the resolving cysteine to form a disulfide bond [19], subsequently reduced by thioredoxin [21]. However, at high levels H_2O_2 can further react with the peroxidatic Cys-SOH, prior to its condensation with the resolving Cys-SH, oxidizing it into the sulfinic acid form (Cys-SO_2H), which inactivates the enzyme [19]. Sulfinylated, inactive Prx is reactivated by reduction by sulfiredoxin (Srx) [22,23], a cytosolic enzyme that translocates into the mitochondrial matrix in response to high H_2O_2 levels to reduce Prx3 [24].

Transcription factor p53 is a master regulator of many forms of cell death [25], and its cytocidal function is often linked to the presence of ROS [26]. In response to oxidative stress, p53 accumulates in the mitochondrial matrix, which causes opening of the mitochondrial permeability transition pore (mPTP), ATP depletion, and necrosis [27]. However, the functional relationship between p53 and ROS in the activation of cell death pathways remains to be elucidated. We have here tested the role of peroxiredoxin 3 and sulfiredoxin, as the major mtROS metabolic system, in the execution of necroptosis by p53 in a murine model of acute pancreatitis [2,28–30].

2. Material and methods

2.1. Animals

Male C57BL/6 and male C57BL/6 *Trp53* null mice (*Trp53*^{tm1Tyj}) were purchased from Jackson Laboratory. One-month old C57BL/6 and *Trp53*^{tm1Tyj} were fed either a standard diet (TD.08485, Envigo, Barcelona, Spain) or a high-fat diet with 42% calories from fat (TD.88137, Envigo, Barcelona, Spain) for 12 weeks. Body weight and food intake were monitored during these 12 weeks. On the other hand, male C57BL/6 *Srxn1* null mice were generated as previously described [31] and were fed standard diet.

All animals were housed under standard environmental conditions (23 ± 1°C, 60% relative humidity, and constant 12 h/12h light/darkness cycles), with food and water *ad libitum,* at the animal housing facilities from the SCSIE located at the Faculty of Pharmacy from the Universitat de València. All procedures and experiments were conducted in compliance with the legislation on protection of animals used for scientific purposes in Spain (RD 53/2013) and the EU (Directive 2010/63/EU). The study was approved by the Ethics Committee of Animal Experimentation and Welfare of the University of Valencia (Valencia, Spain) (Protocol codes: 2020/VSC/PEA/0030; 2020/VSC/PEA/0030; and 2021/VSC/PEA/0216).

2.2. Experimental model of acute pancreatitis

Acute pancreatitis was induced in 16–18-week-old mice fed standard diet by seven intraperitoneal injections of cerulein (Sigma-Aldrich, St. Louis, MO, USA) (50 μg/kg body weight) at 1 h intervals. Physiological saline (0.9% NaCl) was administered to the control group. Animals were sacrificed 1 h after the first, third, fifth and seventh injections of cerulein (i.e., 1, 3, 5, and 7 h after the first cerulein injection) or 18 h after the seventh injection of cerulein (i.e., 24 h after the first cerulein injection) depending on the design of the study. For the sacrifice, mice were anesthetized by inhalation of isoflurane 3–5% and exsanguinated by cardiac puncture followed by cervical dislocation. The blood was collected, and the pancreas was immediately removed and processed according to the protocol used in the different determinations.

In one group of wild-type mice fed standard diet, a solution containing necrostatin-1 (Sigma-Aldrich, St. Louis, MO, USA) and GSK872 (Sigma-Aldrich, St. Louis, MO, USA) dissolved in phosphate-buffered saline with 5% DMSO was administered intraperitoneally (1 mg/kg necrosatin; 1 mg/kg GSK872) 1 h after the seventh injection of cerulein. In another group of SRX KO mice, the mitochondrial antioxidant mito-TEMPO (Sigma-Aldrich, St. Louis, MO, USA) was administered intraperitoneally (25 mg/kg body weight) 10 min before the first and fourth cerulein injection.

2.3. Western blot

Pancreatic tissues were frozen at −80 °C until homogenization in extraction buffer (100 mg/ml) on ice. The protein extraction buffer contained 20 mM Tris–HCl (pH 7.5), 1 mM EDTA, 150 mM NaCl, 0.1% SDS, 1% Igepal CA-630, 30 mM sodium pyrophosphate, 50 mM sodium fluoride, 50 μM sodium orthovanadate (all from Sigma-Aldrich, St. Louis, MO, USA) and a protease inhibitor cocktail (Sigma-Aldrich, St. Louis, MO, USA) at a concentration of 4 μl/mL. After homogenization, the extract was centrifuged at 15.000 g for 15 min, the pellet was discarded, and protein concentration was determined by bicinchoninic acid (BCA) assay in the supernatant. Equal amounts of protein (20–40 μg) were added to sample buffer (62.5 mM Tris–HCl, pH 6.8, 10% glycerol, 0.005% bromophenol blue, 1% SDS, and 50 mM DTT, all from Sigma-Aldrich, St. Louis, MO, USA) with a ratio for sample and buffer of 3:1, and then the mixture was boiled for 5 min at 95 °C. Subsequently, proteins were separated in SDS-PAGE gel (gel percentage was selected depending on the size of the protein of interest) under constant voltage (120–150 V) and were transferred onto nitrocellulose membrane using Trans-Blot® Turbo™ Transfer System (Bio-Rad Laboratories, Hercules, CA, USA) for 20 min at 120 V. Membranes were then incubated for 1 h in blocking buffer to avoid non-specific antibody binding. Blocking buffer consisted in 5% bovine serum albumin in TBS-T (0.1% Tween-20, 20 nM Tris, 137 mM NaCl, pH 7.6). After the blocking step, the membrane was incubated overnight at 4 °C with the suitable primary antibody (Supplementary Table 1) to detect the protein of interest. After incubation with the primary antibody, the membrane was washed three times with TBS-T, and then incubated with secondary antibody conjugated with horseradish peroxidase (Supplementary Table 2) for 1 h at room temperature. After that, the membrane was washed again three times with TBS-T and it was incubated with Pierce™ ECL Western Blotting Substrate (Thermo Fisher Scientific, Rockford, IL, USA) for 5 min at room temperature. Chemiluminescence was detected with a charge-coupled device camera Biorad ChemiDoc™ XRS + Molecular Imager (Bio-Rad Laboratories, Hercules, CA, USA) and LAS-3000 (Fujifilm, Minato-ku, Tokyo, Japan).

2.4. Mitochondria isolation and extraction of mitochondrial proteins

Mitochondrial isolation from pancreatic tissue was performed using Mitochondria Isolation Kit for Tissue (Thermo Fisher Scientific, Rockford, IL, USA). In order to extract mitochondrial proteins for subsequent analysis by western blot, isolated mitochondria were lysed with 2% CHAPS in Tris buffered saline (25 mM Tris, 0.15 M NaCl; pH 7.2). The lysate was centrifuged at 10,000 g for 2 min and then, the supernatant containing soluble mitochondrial proteins was obtained for analysis by western blot.

2.5. H_2O_2 and superoxide measurements

The Amplex Red Hydrogen Peroxide/Peroxidase kit (Thermo Fisher Scientific, Rockford, IL, USA) was used to measure H_2O_2 levels in pancreas. For this purpose, pancreas was homogenized in PBS and hydrogen peroxide levels were measured by fluorimetry according to the manufacturer's instructions. The fluorescence signal was detected with excitation at 530 nm and emission at 590 nm using Fluoroskan Ascent FL™ Microplate Fluorometer (Thermo Fisher Scientific, Rockford, IL, USA).

Mitochondrial H_2O_2 generation was measured in isolated mitochondria in the assay buffer containing 125 mM KCl, 2 mM KH_2PO_4, 2 mM $MgCl_2$, 20 mM Hepes, 0.25 mM EGTA, 0.5 mg/ml fatty acid free BSA, pH 7 at 37 °C, in the presence of exogenous superoxide dismutase (40 U/ml), horseradish peroxidase (HRP) (0.2 U/ml) and Amplex Red (10 μM), and the respiratory substrates (5 mM pyruvate + malate, 5 mM succinate or 5 mM succinate + 0,5 μM rotenone) at 37 °C. The fluorescent intensity of resorufin, the oxidized product of amplex red, was monitored kinetically using Fluoroskan Ascent FL™ Microplate Fluorometer (Thermo Fisher Scientific, Rockford, IL, USA) at excitation 530 nm and emission 590 nm.

Mitochondrial superoxide levels were measured in intact isolated mitochondria in Hank's balanced salt solution with calcium and magnesium (HBSS/Ca^{2+}/Mg^{2+}) containing 5 μM MitoSOX™ (Thermo Fisher Scientific, Rockford, IL, USA) and the respiratory substrates (5 mM pyruvate + malate, 5 mM succinate or 5 mM succinate + 0,5 μM rotenone). The fluorescent intensity was detected at 20 min of incubation using Fluoroskan Ascent FL™ Microplate Fluorometer (Thermo Fisher Scientific, Rockford, IL, USA) at excitation 510 nm and emission 580 nm, as previously described [32].

2.6. Quantitative real-time PCR (RT-qPCR)

A piece of around 30 mg of pancreas was excised, immediately immersed in RNA-later solution (Ambion, Thermo Fisher Scientific, Rockford, IL, USA) to stabilize the RNA, and homogenized in 500 μl of TRIzol™ Reagent (Thermo Fisher Scientific, Rockford, IL, USA). The extract was centrifuged for 10 min at 10,000 g and 4 °C, the pellet was discarded and 100 μl of chloroform was added to the supernatant. The aqueous phase was collected, mixed with 250 μl of isopropanol, incubated for 10 min at room temperature, and then centrifuged at 10,000g for 10 min at 4 °C to precipitate RNA. The supernatant was removed, and the pellet was dissolved in 500 μl of cold 75% ethanol. After centrifugation at 7500 g for 5 min at 4 °C, the pellet was dissolved in 25 μl of Nuclease-Free Water (Ambion, Thermo Fisher Scientific, Rockford, IL, USA). The concentration and purity of RNA were determined using NanoDrop™ Lite Spectrophotometer (Thermo Fisher Scientific, Rockford, IL, USA). To assess the quality of the RNA, isolated RNA (2 mg/lane) was size-fractionated by electrophoresis in a 1% agarose/formalin gel, and stained with GelRed® Nucleic Acid Gel Stain (Biotium, Landing Parkway Fremont, CA, USA).

Once RNA was isolated, reverse transcription was performed to obtain the complementary DNA sequences using PrimeScript™ RT Reagent Kit (Takara, Shiga, Japan) according to the manufacturer's instructions in a C1000 Thermal Cycler (Bio-Rad, California, USA). RT-qPCR was carried out using an iQ™5 Multicolor Real-Time PCR Detection System (Bio-Rad, California, USA) thermal cycler coupled to fluorescence detection. Every reaction was performed in triplicate and melt curves were analyzed with iQ™ Real Time Detection System Software (Bio-Rad, California, USA) to check that only one PCR product per sample was formed. Specific oligonucleotides were designed and synthesized by Sigma-Aldrich, St. Louis, MO, USA (Supplementary Table 3). The efficiency of each pair of primers (1.9–2.1) was checked using a standard curve of cDNA concentration. The RNA level was analyzed by dsDNA binding dye SyberGreen PCR Master mix (Takara, Kusatsu, Shiga, Japan) in an iQTM5 Multicolor Real-Time PCR Detection System (Biorad Laboratories, Hercules, CA, USA). The amplification conditions were 10 min at 95 °C and 40 cycles of 15 s at 95°C, 30 s at 60–64°C (according to the optimal temperature of oligonucleotide hybridization) and 30 s of elongation at 72 °C. Relative mRNA expression was calculated taking into account the threshold cycle from each gene according to the following formula: $2^{-\Delta(\Delta CT)}$, where $\Delta C_T = C_T$ target – C_T housekeeping, and $\Delta(\Delta CT) = \Delta C_T$ treated - ΔC_T control. *Tbp* was used as housekeeping gene to normalize the transcription analysis.

2.7. Measurements of plasma cell free DNA, MLKL and HMGB1 levels

For measurement of plasma cell free DNA (cfDNA), 50 μl of plasma were added to a 96-well plate followed by addition of 50 μl of Sytox Green (1 μM in PBS) (Thermo Fisher Scientific, Rockford, IL, USA). Plates were read immediately at 485/528 nm excitation/emission wavelengths using Fluoroskan Ascent FL™ Microplate Fluorometer (Thermo Fisher Scientific, Rockford, IL, USA).

A mouse MLKL enzyme-linked immunosorbent assay (ELISA) kit (LSBio, Inc., Seattle, WA, USA) and a mouse HMGB1 ELISA kit (Cloud Clone Corp, Katy, TX, USA) were used to measure plasma MLKL and HMGB1 levels, respectively, following the instructions of the kits.

2.8. Histological analysis

Pancreatic specimens were removed and fixed in freshly prepared 4% paraformaldehyde (PFA). After 24 h of fixation in PFA, samples were sent to the Microscopy Section at the SCSIE from the Universitat de València for paraffin embedding. Then, 4 μm sections were prepared using an automatic microtome and stained with hematoxylin-eosin. At least 10 random fields per tissue sample were observed under the brightfield microscope. The extent and severity of necrosis were assessed blindly using a scale ranging from 0 to 3 as previously described [33].

2.9. Statistical analysis

The results were expressed as mean ± standard deviation. Comparisons between 2 groups were made using unpaired 2-tailed *t*-test. Comparison between multiple groups was made using 1- or 2-way ANOVA followed by Bonferroni's or Tukey's test to investigate differences between the individual groups. $P \leq 0.05$ was considered as statistically significant.

3. Results

3.1. A mouse model of necroptosis in acute pancreatitis

We first sought to identify the occurrence of necroptosis in mice with cerulein-induced acute pancreatitis. Mice were given seven times, every hour, cerulein (50 μg/kg) intraperitoneally and were sacrificed 7 h and 24 h after the first injection. Relative levels of phospho-MLKL in the pancreas, used as a marker of necroptosis, did not change at 7 h but were dramatically increased at 24 h, relative to control mice (Fig. 1a and Supplementary Fig. S1a). Necrotic and necroptotic cell death cause the cellular release of DNA or chromatin-associated proteins, such as the high mobility group box 1 (HMGB1) protein [34], and the release of MLKL into the circulation, also a specific marker of necroptosis [35]. We thus measured the levels of cfDNA, HMGB1 and MLKL in the plasma of mice with acute pancreatitis 7 h and 24 h after the first cerulein injection. cfDNA and MLKL plasma levels did not change at 7 h, but exhibited a marked increase at 24 h (Fig. 1b and c), thus paralleling the phosphorylation of MLKL, in contrast to HMGB1 plasma levels that remained unchanged at both time points (Fig. 1d). To verify whether the increased cfDNA levels originated from necroptosis, we treated mice with the RIPK1 and RIPK3 inhibitors necrostatin-1 and GSK872, respectively, at the time of injecting the first cerulein dose, and collected pancreatic tissues 24 h later. Inhibition of RIPK1 and RIPK3 prevented the phosphorylation of pancreatic MLKL (Fig. 1e and Supplementary Fig. S1b), and also diminished necrotic/necroptotic cell death in the pancreas, as showed by the histological analysis of the pancreas (Fig. 1f). Importantly, plasma cfDNA levels were also much lower after the treatment with necroptosis inhibitors, with no statistical differences between inhibitor-treated mice with pancreatitis and control mice without pancreatitis (Fig. 1g). Therefore, we may conclude that the increase in plasma cfDNA was specifically associated with necroptosis during acute pancreatitis. Plasma levels of both cfDNA and MLKL can thus serve as

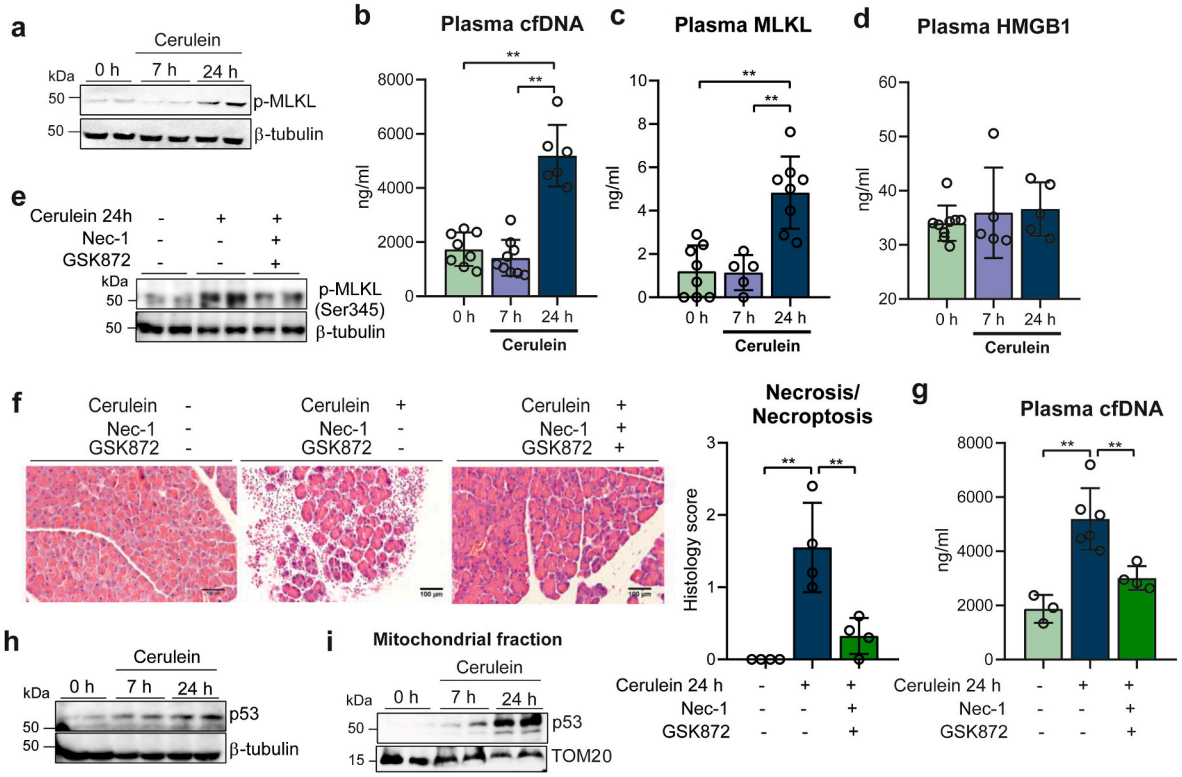

Fig. 1. **a,** Representative western blot showing p-MLKL protein levels in pancreas from control mice at 0 h and from mice with acute pancreatitis at 7 h and 24 h after the first cerulein injection. β-tubulin was used as loading control. **b,** Plasma levels of cell free DNA (cfDNA), **c,** MLKL, and **d,** HMGB1 in control mice at 0 h, and in mice with acute pancreatitis at 7 h and 24 h after the first cerulein injection. **e,** Representative western blot showing p-MLKL protein levels in pancreas from control mice, from mice with acute pancreatitis 24 h after the first cerulein injection, and from mice with acute pancreatitis 24 h after the first cerulein injection treated with Nec-1 and GSK872. β-tubulin was used as loading control. **f,** Representative histological images of hematoxylin-eosin staining and histological score for necrosis of pancreas from control mice, from mice with acute pancreatitis 24 h after the first cerulein injection, and from mice with acute pancreatitis 24 h after the first cerulein injection treated with Nec-1 and GSK872 (Scale bar, 100 μm). **g,** Plasma levels of cell free DNA (cfDNA) in control mice, in mice with acute pancreatitis 24 h after the first cerulein injection, and in mice with acute pancreatitis 24 h after the first cerulein injection treated with Nec-1 and GSK872. **h,** Representative western blot showing p53 protein levels in pancreas from control mice at 0 h and from mice with acute pancreatitis at 7 h and 24 h after the first cerulein injection. β-tubulin was used as loading control. **i,** Representative western blot of p53 protein levels in mitochondrial fraction of pancreas from control mice at 0 h and from mice with acute pancreatitis at 7 h and 24 h after the first cerulein injection. TOM20 was used as loading control. Data are presented as mean ± SD, **P < 0.005, *P < 0.05 (one-way ANOVA, followed by Tukey's multiple comparisons test).

markers of necroptosis in cerulein-induced acute pancreatitis, as they correlate with the activation of pancreatic necroptosis.

3.2. p53 deficiency prevents necroptosis during acute pancreatitis

To assess the role of p53 in necroptosis during acute pancreatitis, we first monitored its protein levels in both total pancreatic tissues and their mitochondrial fraction. p53 levels in whole pancreatic tissue increased at 24 h, but remarkably p53 was detected in the mitochondrial fraction as soon as at 7 h after the first cerulein injection, and its levels further increased at 24 h (Fig. 1h and Supplementary Fig. S1c), (Fig. 1i and Supplementary Fig. S1d). To further evaluate the role of p53, we induced acute pancreatitis in p53 KO mice. The increase in phospho-MLKL levels seen in wild-type animals with acute pancreatitis was absent in p53 KO mice (Fig. 2a and Supplementary Fig. S2a). In addition, plasma levels of cfDNA and of MLKL did not increase in p53 KO (Fig. 2b and c), and pancreatic histologic features diagnostic of necrotic/necroptotic cell death were significantly decreased in p53 KO mice, relative to wild-type mice (Fig. 2d). MLKL plasma levels also remained low in p53 KO mice (Fig. 2c). We conclude here that p53 is required for the occurrence of necroptosis during acute pancreatitis.

3.3. p53-dependent necroptosis associates with increased H_2O_2 via downregulation of sulfiredoxin and peroxiredoxin 3

To explore the possible role of mitochondrial ROS and its functional linkage to p53 in the occurrence of necroptosis, we explored the status of Prx3 as the major mitochondrial H_2O_2 scavenging enzyme, along with its cognate cysteine sulfinic acid reductase Srx, and of PGC-1α, a master regulator of mitochondrial antioxidant defense that also regulates Prx3. We first monitored their expression in the pancreas of wild type and p53 KO mice. Strikingly, both PGC-1α and Srx1 protein levels were significantly increased in sham p53 deficient mice, while these proteins were both barely detectable in sham wild type animals (Fig. 2e and f, and Supplementary Figs. S2b and S2c). PGC-1α and Srx1 protein levels further increased 24 h after cerulein injection in p53 deficient mice, but not in control mice. In sham p53 KO mice, the mRNA and protein levels of Prx3 were also elevated, relative to wild type, and slightly increased 24h after cerulein injection, but not in sham control mice (Fig. 2g and h, and Supplementary Fig. S2d).

By causing upregulation of major mitochondrial ROS defense mechanisms, p53 deficiency may thus protect the organelle from ROS toxicity, and as a corollary, p53 may induce necroptosis by enhancing mitochondrial ROS. To further evaluate this hypothesis, we monitored in the same mice the level of sulfinylation of mitochondrial located Prx3, as a faithful indication of increased mitochondrial matrix H_2O_2 levels, using cytosolic PRX1/2 as control. We used an anti-Cys-SO_2/SO_3 that

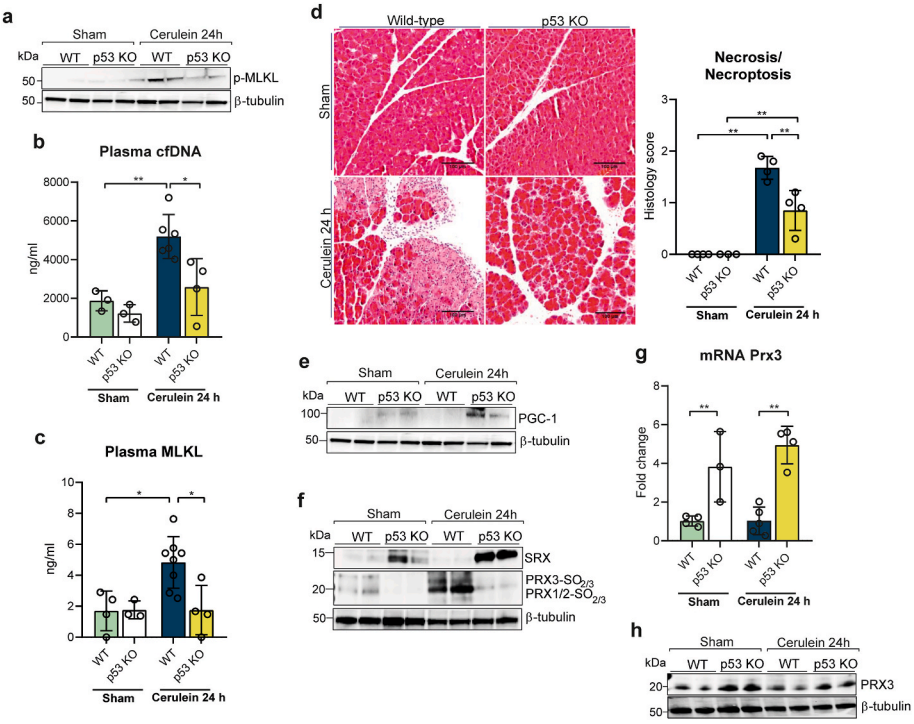

Fig. 2. a, Representative western blot of p-MLKL protein levels in pancreas from wild-type (WT) and p53 knockout (KO) mice under basal conditions (sham) and with acute pancreatitis at 24 h after the first cerulein injection. β-tubulin was used as loading control. **b,** Plasma levels of cell free DNA (cfDNA) and **c,** plasma levels of MLKL in wild-type (WT) and p53 knockout (KO) mice under basal conditions (sham) and with acute pancreatitis at 24 h after the first cerulein injection. **d,** Representative histological images of hematoxylin-eosin staining and histological score for necrosis of pancreas from wild-type (WT) and p53 knockout (KO) mice under basal conditions (sham) and with acute pancreatitis at 24 h after the first cerulein injection (Scale bar, 100 μm). **e,** Representative western blot of PGC-1α, **f,** SRX and hyperoxidized forms of PRX1, PRX2 and PRX3 protein levels in pancreas from wild-type (WT) and p53 knockout (KO) mice under basal conditions (sham) and with acute pancreatitis at 24 h after the first cerulein injection. β-tubulin was used as loading control. **g,** mRNA relative expression of *Prx3 vs. Tbp* in pancreas from wild-type (WT) mice and p53 knockout (KO) mice under basal conditions (sham) and with acute pancreatitis at 24 h after the first cerulein. **h,** Representative western blot of PRX3 protein levels in pancreas from wild-type (WT) and p53 knockout (KO) mice under basal conditions (sham) and with acute pancreatitis at 24 h after the first cerulein injection. β-tubulin was used as loading control. Data are presented as mean ± SD, **P < 0.005, *P < 0.05 (two-way ANOVA, followed by Tukey's multiple comparisons test).

distinguishes Prx3 from Prx1/2 because of the different size of these enzymes, but not Prx1 and Prx2 that are of same size [24]. In the pancreas of sham wild type mice, background sulfinylation signals were seen for Prx1/2, but not for Prx3; 24 h after cerulein injection these signals dramatically increased with the appearance of a Prx3 sulfinylation signal. In striking contrast, in sham p53 KO mice no sulfinylation signals were seen for any of the peroxiredoxins, despite the presence of these enzymes (Fig. 2f and Supplementary Fig. S2e), as shown for Prx3 (Fig. 2h and Supplementary Fig. S2d), and 24 h after cerulein injection only a very weak Prx1/2 sulfinylation signal was seen (Fig. 2f and Supplementary Fig. S2e).

In keeping with the high sulfinylation levels of all three Prx enzymes in the inflammatory pancreas, H_2O_2 levels were elevated in mitochondria isolated from pancreatic tissue of wild type mice suffering from pancreatitis relative to wild type control mice, in contrast to superoxide that remained without changes (Supplementary Figs. S2f and S2g). We conclude here that murine acute pancreatitis associates with a high production of cellular and mitochondrial H_2O_2, which is largely mitigated in p53-deficient mice presumably due to the up-regulation of Srx and at a lower degree of Prx3. Furthermore, these data suggest that during acute pancreatitis p53 triggers necroptosis by a H_2O_2-dependent mechanism via downregulation of Srx and Prx3.

3.4. Mitochondrial translocation of sulfiredoxin occurs early during acute pancreatitis in association with enhanced H_2O_2 generation

The striking difference between wild type and p53-deficient mice in both the expression of Srx and the accumulation of sulfinylated Prxs in pancreas led us to carefully explore the expression of Srx, its subcellular localization, and Prx sulfinylation in pancreas from wild type mice during the course of cerulein-induced acute pancreatitis. Relative to control mice under basal conditions, *Srxn1* mRNA and Srx protein levels increased 7 h after cerulein injection, at a time where phospho-MLKL had not yet increased (see Fig. 3a and Supplementary Fig. S1a), returning to pre-treatment levels at 24 h, when phospho-MLKL was present (Fig. 3a and b). We also monitored the kinetics of *srxn1* induction at early time points after injection, showing that *srxn1* mRNA levels peaked 5 h after the first cerulein injection (~170 fold increase) (Fig. 3c). Srx protein levels paralleled the *srxn1* levels changes, reaching a maximum at time 7 h (~3 fold) (Fig. 3d). To assess the sulfinic acid reductase activity during this time period, we monitored in parallel the sulfinylation of its substrates PRX1/PRX2 and PRX3, together with the H_2O_2 levels in the pancreas. Remarkably, all three peroxiredoxins appeared highly sulfinylated as early as 1 h, returning to pre-treatment levels at 5 h; sulfinylation of Prx1/2, but not Prx3, increased again at 7 h (Fig. 3e). H_2O_2 levels peaked at 1h, decreased afterwards to increase again up to 7 h (Fig. 3f), thus matching these two H_2O_2 waves the accumulation of Prxs in their sulfinylated form. Srx translocates to mitochondria in a redox- and Hsp90-dependent manner when mitochondrial matrix H_2O_2 levels are elevated [24]. Accordingly and importantly, Srx was almost totally localized to the mitochondria at 7 h after cerulein injection (Fig. 3g).

We conclude here that H_2O_2 is produced by the pancreas during the course of acute pancreatitis in two waves, the first at 1 h that originates, at least in part, in mitochondria, as suggested by the sulfinylation of Prx3 and the mitochondrial localization of Srx, and the second wave starting at 7 h after initiation of the disease, of non-mitochondrial origin.

3.5. Sulfiredoxin deficiency exacerbates mitochondrial translocation of p53 and necroptosis in acute pancreatitis

The very high upregulation of Srx and almost absence of Prx sulfinylation in necroptosis-resistant p53 KO mice (see Fig. 2), together with the high mitochondrial production of H_2O_2 early in the course of the disease led us to explore the role of Srx, using *srxn1* KO mice. We monitored the pancreas of these mice 7 h after cerulein injection, the time at which Srx was maximally induced in wild type animals. In *srxn1* KO mice, phosphorylation of MLKL in pancreatic tissues was already

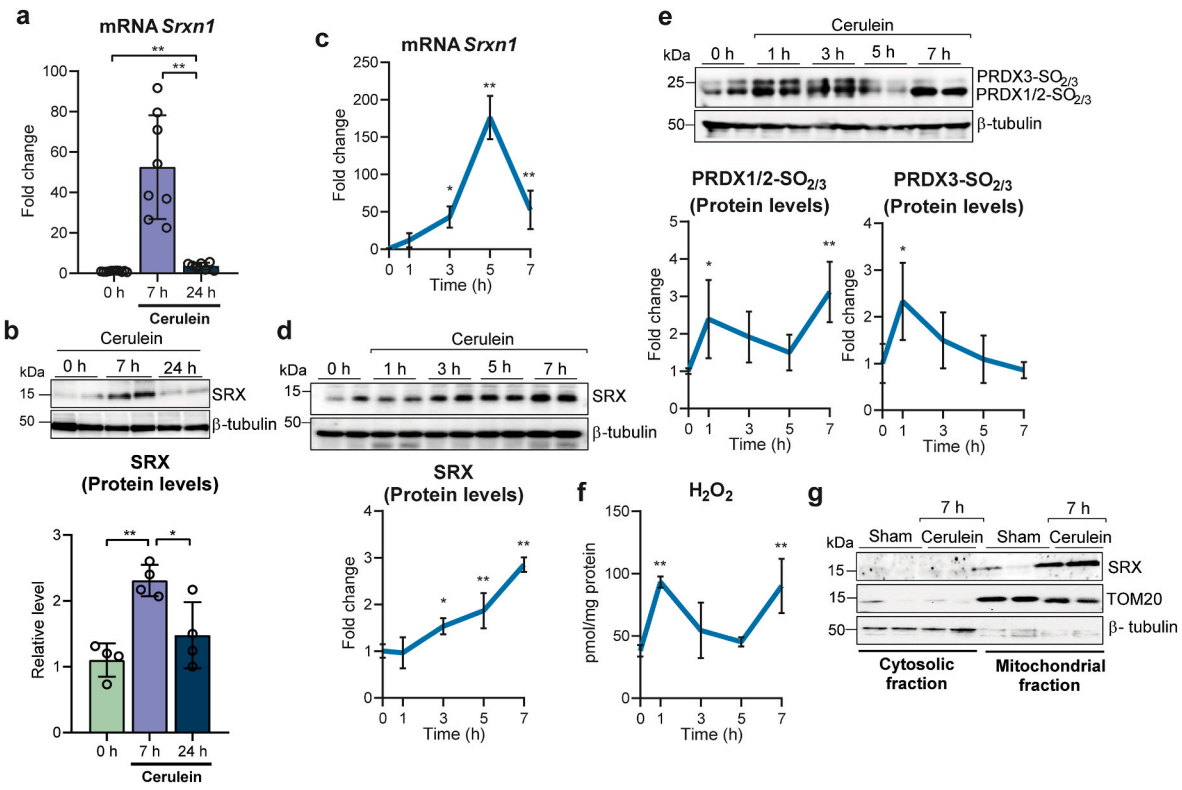

Fig. 3. a, mRNA relative expression of *Srxn1 vs. Tbp* in pancreas from control mice at time 0 h and from mice with acute pancreatitis 7 h and 24 h after the first cerulein injection. Data are presented as mean ± SD, **P < 0.005 (one-way ANOVA, followed by Tukey's multiple comparisons test). **b,** Representative western blot and densitometry quantification showing SRX protein levels in pancreas from control mice at 0 h and from mice with acute pancreatitis at 7 h and 24 h after the first cerulein injection. β-tubulin was used as loading control. **c,** mRNA relative expression of *Srxn1 vs. Tbp* in pancreas from control mice at 0 (n = 6), 1 (n = 3), 3 (n = 3), 5 (n = 3), and 7 h (n = 8) after the first cerulein injection. **d,** Representative western blot and densitometry quantification of SRX protein levels in pancreas from control mice at 0, 1, 3, 5, and 7 h after the first cerulein injection (n = 4 mice per group). β-tubulin was used as loading control. **e,** Representative western blot and densitometry quantification showing hyperoxidized forms of PRX1, PRX2 and PRX3 in pancreas from control mice at 0, 1, 3, 5, and 7 h after the first cerulein injection (n = 4 mice per group). β-tubulin was used as loading control. **f,** Levels of H_2O_2 in pancreas from control mice at 0 (n = 4), 1 (n = 3), 3 (n = 3), 5 (n = 3), and 7 h (n = 8) after the first cerulein injection. **g,** Representative western blot of SRX in cytosolic and mitochondrial fraction of pancreas from sham mice and at 7 h after the first injection of cerulein (n = 4 mice per group). TOM20 was used as loading control for mitochondrial fraction. β-tubulin was used as loading control for cytosolic fraction. Data are presented in panels **c-f** as mean ± SD, **P < 0.005, *P < 0.05 (each time point *vs.* control mice at time 0 by one-way ANOVA, followed by Bonferroni's multiple comparisons test).

intense at 7h, but was not yet detected in wild type controls (Fig. 4a and Supplementary Fig. S3a), and plasma levels of cfDNA and MLKL were elevated only in Srx-deficient mice (Fig. 4b and c). Pancreatic histological inspection revealed that necrosis/necroptosis was greatly enhanced in *srxn1* KO mice, relative to wild type mice (Fig. 4d).

The intense necroptosis seen in *srxn1* KO mice, which occurred very early during the disease, was associated with an elevation of mitochondrial H_2O_2 that lasted up to 7 h, as evidenced by the intense hyperoxidation of Prx3, along with that of Prx1/Prx2 (Fig. 4e and Supplementary Figs. S3b and S3c). Such an increase in mitochondrial H_2O_2 was also manifested by marked generation of reactive nitrogen species, as indicated by the presence of nitrated proteins in mitochondria at much higher levels than those seen in wild type mice (Fig. 4f, see also Fig. 3e).

Lastly, p53 was already strongly induced 7 h after cerulein injection in srxn1 KO mice, much earlier than in wild type mice (see Fig. 1h and Supplementary Fig. S1c), as shown by an increase in the levels of p53 mRNA and protein and by a significant accumulation of the protein in mitochondria (Fig. 4f, g, h, and Supplementary Figs. S3d and S3e).

3.6. Mito-TEMPO abrogates necroptosis in SRX-deficient mice with acute pancreatitis

All our above data suggested that early during the course of pancreatitis, mitochondrial H_2O_2 production and mitochondrial p53 translocation combine to trigger necroptosis, with p53 also exacerbating mitochondrial H_2O_2 levels by down-regulating the expression of Srx and Prx3. To further demonstrate the critical role of mitochondrial H_2O_2 in necroptosis execution, already supported by the Srx KO model, we enquired whether the mitochondrial antioxidant mito-TEMPO could diminish or prevent the necroptosis of acute pancreatitis in *srxn1* KO mice, when administered at the time of the first cerulein injection. At 7 h after the first cerulein injection, mito-TEMPO significantly decreased both p53 mRNA levels and the accumulation of p53 in mitochondria (Fig. 5a and b and Supplementary Fig. S3f). Mito-TEMPO also prevented the increase in pancreatic p-MLK levels (Fig. 5c and Supplementary Fig. S3g) as well as in plasma cfDNA and MLKL levels (Fig. 5d and e). Histological inspection also showed that mito-TEMPO significantly decreased the features of necrotic/necroptotic cell death seen in srxn1 KO mice that did not receive the antioxidant (Fig. 5f). Altogether, these data suggest that mitochondrial H_2O_2 production has a critical role in the trigger of necroptosis mediated by p53.

3.7. p53 is required for necroptosis in the pancreas and adipose tissue of obese mice

We sought to evaluate whether the mitochondrial H_2O_2- and p53-dependent necroptotic pathway that occurs during acute pancreatitis was relevant to other models of necroptosis and to other tissues. We chose the necroptosis associated with obesity induced by high fat diet, as

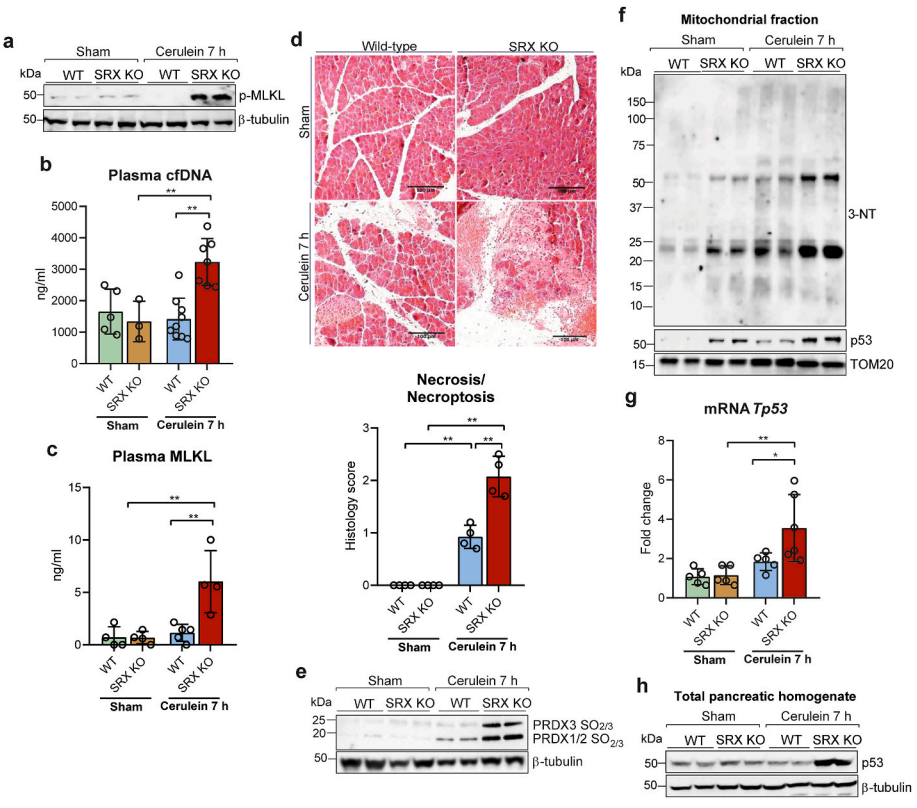

Fig. 4. a, Representative western blot of p-MLKL protein levels in pancreas from wild-type (WT) and SRX knockout (KO) mice under basal conditions (sham) and with acute pancreatitis at 7 h after the first cerulein injection. β-tubulin was used as loading control. **b,** Plasma levels of cell free DNA (cfDNA) and **c,** plasma levels of MLKL in wild-type (WT) and SRX knockout (KO) mice under basal conditions (sham) and with acute pancreatitis at 7 h after the first cerulein injection. **d,** Representative histological images of hematoxylin-eosin staining and histological score for necrosis of pancreas from wild-type (WT) and SRX knockout (KO) mice under basal conditions (sham) and with acute pancreatitis at 7 h after the first cerulein injection (Scale bar, 100 μm). **e,** Representative western blot of hyperoxidized forms of PRX1, PRX2 and PRX3 in pancreas from wild-type (WT) and SRX knockout (KO) mice under basal conditions (sham) and with acute pancreatitis at 7 h after the first cerulein injection. β-tubulin was used as loading control. **f,** Representative western blot of 3-nitrotyrosine and p53 levels in mitochondrial fraction of pancreas from wild-type (WT) and SRX knockout (KO) mice under basal conditions (sham) and with acute pancreatitis at 7 h after the first cerulein injection. TOM20 was used as loading control. **g,** mRNA relative expression of *Tp53 vs. Tbp* in pancreas from wild-type (WT) mice and SRX knockout (KO) mice under basal conditions (sham) and with acute pancreatitis at 7 h after the first cerulein. **h,** Representative western blot of p53 protein levels in pancreas from wild-type (WT) and SRX knockout (KO) mice under basal conditions (sham) and with acute pancreatitis at 7 h after the first cerulein injection. β-tubulin was used as loading control. Data are presented in panels **b, c, d** and **g** as mean ± SD, **P < 0.005, *P < 0.05 (two-way ANOVA, followed by Tukey's multiple comparisons test).

obesity causes PGC-1α deficiency in the pancreas [36], the loss of which may promote ROS- and p53-dependent necroptosis. Strikingly, p53 was present at significant levels in pancreatic mitochondria from obese mice, but not in those from lean mice (Fig. 6a and Supplementary Fig. S4a), which suggests that p53 might be triggering the pancreatic necroptosis that we expected in obese mice. In keeping with the later hypothesis, MLKL phosphorylation was also high in pancreas from obese mice relative to lean mice, in which this necroptotic marker was almost undetectable (Fig. 6c and Supplementary Fig. S4b). MLKL phosphorylation was also increased in adipose tissue of obese mice (Fig. 6d and Supplementary Fig. S4c).

We thus checked the effect of p53 deficiency in obese mice. Remarkably, obese p53 KO mice lost the increase in MLKL phosphorylation seen in pancreas and adipose tissue from obese wild type mice (Fig. 6c and d, and Supplementary Figs. S4b and S4c). Surprisingly, p53 KO mice fed high fat diet gained significantly more body weight than their WT littermates, although their body weight was similar when fed standard diet (Supplementary Fig. S4d), a difference that could not be accounted for by changes in daily food intake (Supplementary Figs. S5e and S5f), and thus it might be due either to the lowering level of necroptosis or alternatively to mitochondrial dysfunction associated with reduced β-oxidation.

Prx3 mRNA levels were low in pancreas of both obese wild-type and obese p53 KO mice when compared with lean wild-type and lean p53 KO mice, although the latter exhibited up-regulation of *Prx3* mRNA levels (Fig. 6b). However, as in their lean counterpart, Srx protein levels were also upregulated in pancreas from obese p53 KO mice (Fig. 6, and Supplementary Fig. S4g) in parallel with the prevention of PRX3 hyperoxidation and MLKL phosphorylation (Fig. 6c, and Supplementary Figs. S4b and S4h). Srx protein levels were also increased in adipose tissue from obese p53 KO mice, in agreement with the lack of MLKL phosphorylation (Fig. 6d, and Supplementary Figs. S4c and S4i).

In agreement with these findings, plasma MLKL levels remained very low in obese p53 KO mice similarly to lean mice (Fig. 6e), and cfDNA levels exhibited a much lower increase in obese p53 KO mice than in obese wild-type mice (Fig. 6f). Hence, we conclude here that necroptosis in pancreas and adipose tissue from obese mice is also dependent on p53.

4. Discussion

p53 is a central stress sensor in cells that regulates apoptosis and autophagic cell death, and has been associated with necrosis [27,37,38]. In response to oxidative stress and during brain ischemia/reperfusion injury, p53 accumulates in the mitochondrial matrix and forms a complex with cyclophilin D (CypD) that triggers opening of mitochondrial permeability transition pores (mPTP) and necrosis [27,37]. Moreover, phosphorylated p53 at serine 23 binds CypD in mitochondria to cause necrosis in mouse cortical neurons [39]. Importantly, upon cell stress cytosolic p53 translocates into the mitochondria before exerting its transcriptional activity [40–42]. So far, p53 has been associated with regulated necrosis in mammals only in cardiomyocytes exposed to H_2O_2 and through its transcriptional activity via up-regulation of the long non-coding RNA named necrosis-related factor [43]. In Drosophila p53 is required for the regulated necrosis of mitotic germ cells during normal spermatogenesis [38].

In the present work, we demonstrate that p53 is required for regulated necrosis in acute pancreatitis and in obesity, and additionally we show a new mechanism responsible for p53-mediated necroptosis through the modulation of mitochondrial ROS levels via peroxiredoxin 3 and sulfiredoxin. We have found that in experimental acute pancreatitis, a disease in which the existence of necroptosis in pancreas has been

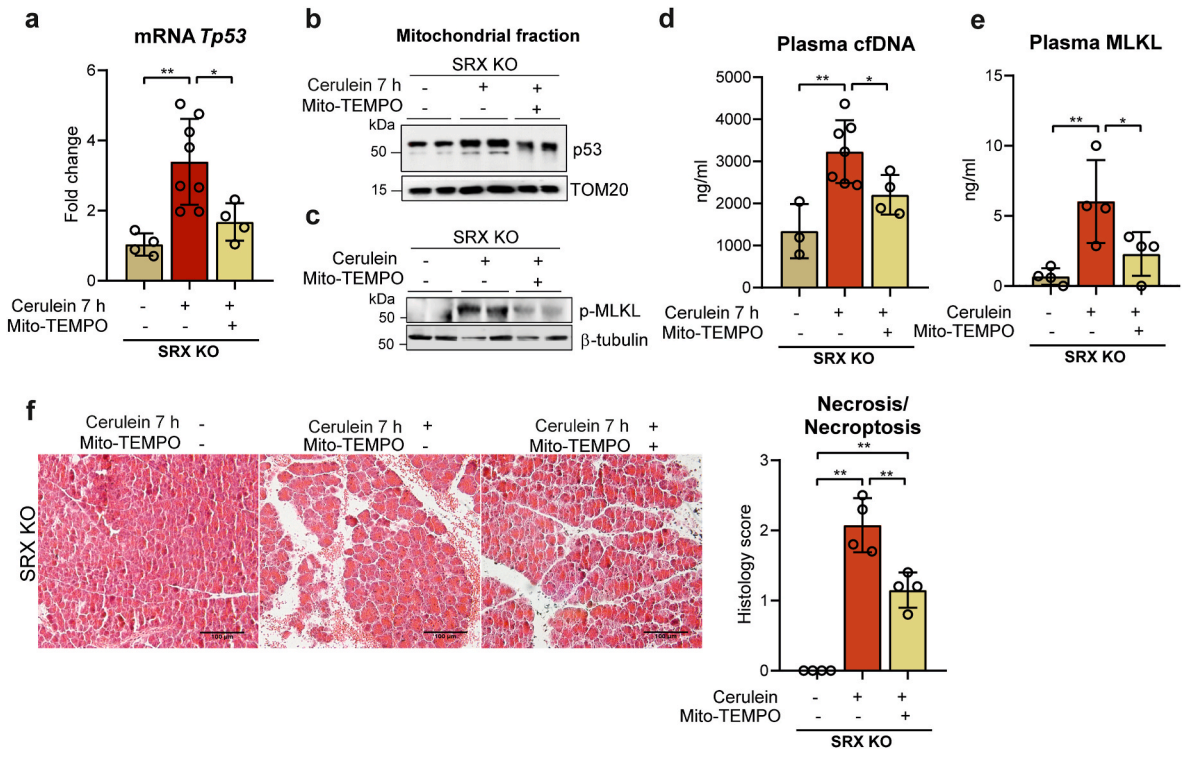

Fig. 5. a, mRNA relative expression of *Tp53 vs. Tbp* in pancreas from SRX KO mice under basal conditions (sham), with acute pancreatitis at 7 h after the first injection of cerulein, and with acute pancreatitis and mito-TEMPO treatment. **b,** Representative western blot of p53 in mitochondrial fraction of pancreas from SRX KO mice under basal conditions (sham), with acute pancreatitis at 7 h after the first injection of cerulein, and with acute pancreatitis and mito-TEMPO treatment. TOM20 was used as loading control. **c,** Representative western blot showing p-MLKL protein levels in pancreas from SRX KO mice under basal conditions (sham), with acute pancreatitis at 7 h after the first injection of cerulein, and with acute pancreatitis and mito-TEMPO treatment. β-tubulin was used as loading control. **d,** Plasma levels of cell free DNA (cfDNA) and **e,** plasma levels of MLKL in SRX KO mice under basal conditions (sham), with acute pancreatitis at 7 h after the first injection of cerulein, and with acute pancreatitis and mito-TEMPO treatment. **f,** Representative histological images of hematoxylin-eosin staining and histological score for necrosis of pancreas from SRX KO mice under basal conditions (sham), with acute pancreatitis at 7 h after the first injection of cerulein, and with acute pancreatitis and mito-TEMPO treatment (Scale bar, 100 μm). Data are presented in panels **a**, **d**, **e**, and **f** as mean ± SD, $^{**}P < 0.005$, $^{*}P < 0.05$ (two-way ANOVA, followed by Tukey's multiple comparisons test).

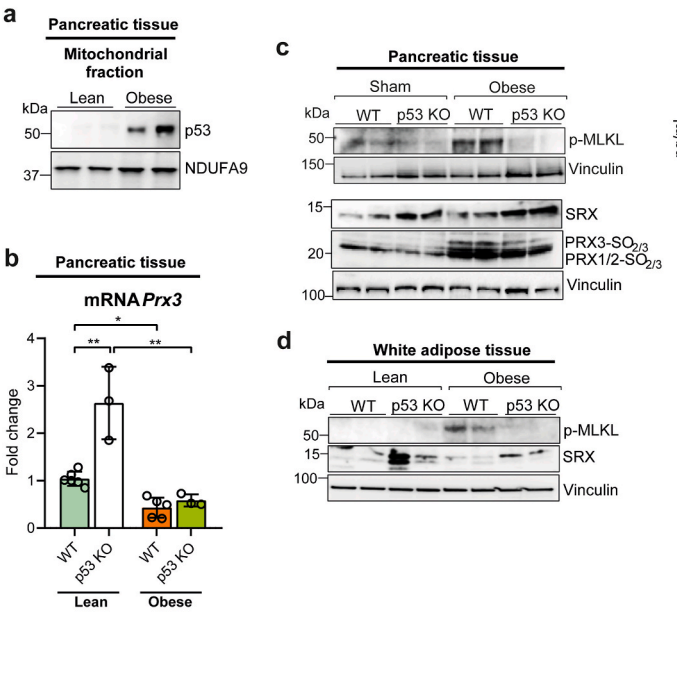

Fig. 6. a, Representative western blot of p53 in mitochondrial fraction of pancreas from lean and obese mice. NDUFA9 was used as loading control. **b,** mRNA relative expression of *Prx3 vs. Tbp* in pancreas from lean and obese wild-type (WT) and p53 knockout (KO) mice. **c,** Representative western blot of phospho-MLKL, SRX, and hyperoxidized forms of PRX1, PRX2 and PRX3 in pancreas from lean and obese wild-type (WT) and p53 knockout (KO) mice. Vinculin was used as loading control. **d,** Representative western blot of phospho-MLKL and SRX in white adipose tissue from lean and obese wild-type (WT) and p53 knockout (KO) mice. Vinculin was used as loading control. **e,** Plasma levels of cell free DNA (cfDNA) and **f,** MLKL in lean and obese wild-type (WT) and p53 knockout (KO) mice. Data are presented in panels **e** and **f** as mean ± SD, $^{**}P < 0.005$, $^{*}P < 0.05$ (two-way ANOVA, followed by Tukey's multiple comparisons test).

confirmed by several authors [2,28–30], mitochondrial translocation of p53 occurs and it is required for the execution of this type of cell death. Indeed, the lack of p53 avoids the phosphorylation of MLKL and importantly, prevents the hyperoxidation of mitochondrial PRX3 through upregulation of SRX, which is critical to prevent the activation of necroptosis. Indeed, SRX is upregulated and translocates into the mitochondria to protect PRX3 from hyperoxidation during the early stage of acute pancreatitis, a period of time during which necroptosis is abrogated. Only when SRX levels drop and PRX3 becomes hyperoxidized, necroptosis occurs. Accordingly, the absence of SRX accelerated the occurrence of necroptosis in pancreas during acute pancreatitis, and remarkably, increased the expression of p53 and its mitochondrial translocation.

Previously, it has been reported that cytosolic SRX translocates into mitochondria to reactivate PRX3 during corticosterone production via formation of a disulfide-linked complex with heat shock protein 90 promoted by mitochondrial H_2O_2 [24,44]. Nevertheless, so far the regulation of PRX3 activity by mitochondrial SRX has not been related to necroptosis. Our results show for the first time an intriguing dual and opposite regulation between p53 and SRX either to delay or accelerate the necroptosis cell death program in acute inflammatory diseases such as acute pancreatitis. mtROS may enhance necrosome formation by promoting the auto-phosphorylation of RIPK1 [16]. In addition, RIPK3 may enhance mtROS generation through activation of the pyruvate-dehydrogenase complex in TNFα-induced necroptosis [18,45].

We show that H_2O_2 is produced by mitochondria very early during the acute pancreatitis process (1 h), as manifested by the accumulation of mitochondrial Prx3 in the sulfinylated form, and the mitochondrial translocation of Srx, and confirmed by increased mitochondrial H_2O_2 levels. Here, we demonstrate that the enhanced generation of mtROS is essential for necroptosis execution and it is critically dependent on p53. It is noteworthy the exacerbation of necroptosis in mice lacking Srx, and furthermore treatment with mito-TEMPO diminishes the upregulation and mitochondrial translocation of p53 and abrogates necroptosis in mice lacking SRX. In p53 KO mice, Prx1/2 and Prx3 never become sulfinylated, which suggests that the upregulation of mitochondrial antioxidant defense seen in these mice efficiently prevents the mitochondrial increase in H_2O_2. Our findings reveal a novel mechanism showing that p53 triggers necroptosis at least in part by promoting a mitochondrial increase in H_2O_2 and the loss of the PRX3 activity, and sulfiredoxin downregulation is a crucial step in the activation of necroptosis. Hence, p53 is located at the crossroad between PRX3/SRX, mtROS, and the necroptosis cascade.

Together with the crosstalk between p53 and SRX/PRX3, we show here that p53 also regulates the levels of PGC-1α, a master regulator of mitochondrial antioxidant defense. Thus, p53 represses PGC1-α, downregulating its transcriptional target PRX3 in pancreas during acute pancreatitis. These results are in agreement with previous findings showing that p53-dependent PGC-1α repression caused cardiomyocyte necrosis and chronic ventricular dysfunction [46]. Therefore, p53 orchestrates the mitochondrial antioxidant response mediated by PGC-1α in acute pancreatitis, which together with the regulation of SRX/PRX3 makes p53 a key regulator of mtROS levels and consequently, a decisive player in necroptosis execution.

In order to confirm the general requirement of p53 for necroptosis, apart from acute inflammation we search for a chronic model of necroptosis such as diet-induced obesity [47]. Thus, we also studied the role of p53 in necroptosis associated with obesity in pancreas and adipose tissue. Our previous work showed that obesity causes a dramatic downregulation of PGC-1α in mouse pancreas [36] and hence, we rationalized that PGC-1α deficiency could lead to down-regulation of its target peroxiredoxin 3 promoting necroptosis in pancreas from obese mice. Indeed, we found peroxiredoxin 3 down-regulation and necroptosis in pancreas from obese mice, and importantly necroptosis was abrogated in obese mice lacking p53. Nevertheless, obese p53 KO mice did not exhibit up-regulation of peroxiredoxin 3 in the pancreas in contrast to what occurred in lean p53 KO mice, which is likely due to the pancreatic PGC-1α deficiency associated with obesity that would keep low peroxiredoxin 3 levels in the pancreas. The occurrence of this pancreatic necroptosis would contribute to the pro-inflammatory condition associated with obesity and also to the related impairment of insulin sensitivity [47]. Similarly, and in agreement with the RIPK3 overexpression found in white adipose tissue in obesity [48], necroptosis occurred in adipose tissue from obese mice. Again and remarkably obese p53 knock out mice did not exhibit necroptosis in adipose tissue, highlighting the key role of p53 as a key mediator of this type of cell death and its relevance in the pathophysiology of obesity. In fact, excessive calorie intake causes an increase in p53 levels in the adipose tissue, which have been related to insulin resistance and the inflammatory response [49,50].

In conclusion, our present findings demonstrate that p53 is required for different models of necroptosis. We also describe here a positive feedback loop between mitochondrial ROS and p53 that is amplified through down-regulation of sulfiredoxin and peroxiredoxin 3 leading to necroptosis in acute inflammation and obesity.

Author contributions

S.R. and S.P performed the experiments and analysis, and participated in the design of the study. J.S. designed the study, and supervised all experiments and analysis. M.B.T provided the sulfiredoxin knock-out mice for this study. J.S. and M.B.T wrote the manuscript.

Declaration of competing interest

There is no conflict of interest.

Data availability

Data will be made available on request.

Acknowledgments

S.R. was recipient of a fellowship from Spanish Ministry of Economy and Competitiveness and from a fellowship Margarita Salas from the Spanish Ministry of Universities. This work was funded by Grants PID2019-108615RB-I00 from the Spanish Ministry of Science and Innovation and SAF2015-71208-R from the Spanish Ministry of Economy and Competitiveness to J.S. both with Feder funds, and from Grant ANR ERRed2 from the Agence Nationale pour la Recherche, France, to M.B.T. The authors also acknowledge scientific advice and guidance for the discussion of the manuscript provided by the Spanish Research Biology and Medicine Redox Network RED2018-102576-T.

Appendix A. Supplementary data

Supplementary data to this article can be found online at https://doi.org/10.1016/j.redox.2022.102423.

References

[1] Y.S. Cho, S. Challa, D. Moquin, R. Genga, T.D. Ray, M. Guildford, F.K. Chan, Phosphorylation-driven assembly of the RIP1-RIP3 complex regulates programmed necrosis and virus-induced inflammation, Cell **137** (2009) 1112–1123.
[2] S. He, L. Wang, L. Miao, T. Wang, F. Du, L. Zhao, X. Wang, Receptor interacting protein kinase-3 determines cellular necrotic response to TNF-alpha, Cell 137 (2009) 1100–1111.
[3] A. Linkermann, D.R. Green, N. Necroptosis, Engl. J. Med. 370 (2014) 455–465.
[4] T. Vanden Berghe, A. Linkermann, S. Jouan-Lanhouet, H. Walczak, P. Vandenabeele, Regulated necrosis: the expanding network of non-apoptotic cell death pathways, Nat. Rev. Mol. Cell Biol. 15 (2014) 135–147.
[5] M. Pasparakis, P. Vandenabeele, Necroptosis and its role in inflammation, Nature 517 (2015) 311–320.
[6] D. Tang, R. Kang, T.V. Berghe, P. Vandenabeele, G. Kroemer, The molecular machinery of regulated cell death, Cell Res. 29 (2019) 347–364.

[7] H. Wang, L. Sun, L. Su, J. Rizo, L. Liu, L.F. Wang, F.S. Wang, X. Wang, Mixed lineage kinase domain-like protein MLKL causes necrotic membrane disruption upon phosphorylation by RIP3, Mol. Cell 54 (2014) 133–146.

[8] Z. Cai, S. Jitkaew, J. Zhao, H.C. Chiang, S. Choksi, J. Liu, Y. Ward, L.G. Wu, Z. G. Liu, Plasma membrane translocation of trimerized MLKL protein is required for TNF-induced necroptosis, Nat. Cell Biol. 16 (2014) 55–65.

[9] Y. Dondelinger, W. Declercq, S. Montessuit, R. Roelandt, A. Goncalves, I. Bruggeman, P. Hulpiau, K. Weber, C.A. Sehon, R.W. Marquis, J. Bertin, P. J. Gough, S. Savvides, J.C. Martinou, M.J. Bertrand, P. Vandenabeele, MLKL compromises plasma membrane integrity by binding to phosphatidylinositol phosphates, Cell Rep. 7 (2014) 971–981.

[10] L. Sun, H. Wang, Z. Wang, S. He, S. Chen, D. Liao, L. Wang, J. Yan, W. Liu, X. Lei, X. Wang, Mixed lineage kinase domain-like protein mediates necrosis signaling downstream of RIP3 kinase, Cell **148** (2012) 213–227.

[11] L. Galluzzi, O. Kepp, F.K. Chan, G. Kroemer, Necroptosis: mechanisms and relevance to disease, Annu. Rev. Pathol. 12 (2017) 103–130.

[12] Z. Wang, H. Jiang, S. Chen, F. Du, X. Wang, The mitochondrial phosphatase PGAM5 functions at the convergence point of multiple necrotic death pathways, Cell **148** (2012) 228–243.

[13] C.W. Davis, B.J. Hawkins, S. Ramasamy, K.M. Irrinki, B.A. Cameron, K. Islam, V. P. Daswani, P.J. Doonan, Y. Manevich, M. Madesh, Nitration of the mitochondrial complex I subunit NDUFB8 elicits RIP1- and RIP3-mediated necrosis, Free Radic. Biol. Med. 48 (2010) 306–317.

[14] N. Vanlangenakker, T. Vanden Berghe, P. Bogaert, B. Laukens, K. Zobel, K. Deshayes, D. Vucic, S. Fulda, P. Vandenabeele, M.J. Bertrand, cIAP1 and TAK1 protect cells from TNF-induced necrosis by preventing RIP1/RIP3-dependent reactive oxygen species production, Cell Death Differ. 18 (2011) 656–665.

[15] Y. Lin, S. Choksi, H.M. Shen, Q.F. Yang, G.M. Hur, Y.S. Kim, J.H. Tran, S. A. Nedospasov, Z.G. Liu, Tumor necrosis factor-induced nonapoptotic cell death requires receptor-interacting protein-mediated cellular reactive oxygen species accumulation, J. Biol. Chem. 279 (2004) 10822–10828.

[16] L. Laurien, M. Nagata, H. Schünke, T. Delanghe, J.L. Wiederstein, S. Kumari, R. Schwarzer, T. Corona, M. Krüger, M.J.M. Bertrand, V. Kondylis, M. Pasparakis, Autophosphorylation at serine 166 regulates RIP kinase 1-mediated cell death and inflammation, Nat. Commun. 11 (2020), 1747-020-15466-8.

[17] Y. Zhang, S.S. Su, S. Zhao, Z. Yang, C.Q. Zhong, X. Chen, Q. Cai, Z.H. Yang, D. Huang, R. Wu, J. Han, RIP1 autophosphorylation is promoted by mitochondrial ROS and is essential for RIP3 recruitment into necrosome, Nat. Commun. 8 (2017), 14329.

[18] A. Sureshbabu, E. Patino, K.C. Ma, K. Laursen, E.J. Finkelsztein, O. Akchurin, T. Muthukumar, S.W. Ryter, L. Gudas, A.M.K. Choi, M.E. Choi, RIPK3 promotes sepsis-induced acute kidney injury via mitochondrial dysfunction, JCI Insight 3 (2018), e98411, https://doi.org/10.1172/jci.insight.98411 eCollection 2018 Jun 7.

[19] S.G. Rhee, I.S. Kil, Multiple functions and regulation of mammalian peroxiredoxins, Annu. Rev. Biochem. 86 (2017) 749–775.

[20] B. Cunniff, A.N. Wozniak, P. Sweeney, K. DeCosta, N.H. Heintz, Peroxiredoxin 3 levels regulate a mitochondrial redox setpoint in malignant mesothelioma cells, Redox Biol. 3 (2014) 79–87.

[21] X. Ren, L. Zou, X. Zhang, V. Branco, J. Wang, C. Carvalho, A. Holmgren, J. Lu, Redox signaling mediated by thioredoxin and glutathione systems in the central nervous system, Antioxidants Redox Signal. 27 (2017) 989–1010.

[22] B. Biteau, J. Labarre, M.B. Toledano, ATP-dependent reduction of cysteine-sulphinic acid by S. cerevisiae sulphiredoxin, Nature 425 (2003) 980–984.

[23] S.G. Rhee, I.S. Kil, Mitochondrial H2O2 signaling is controlled by the concerted action of peroxiredoxin III and sulfiredoxin: linking mitochondrial function to circadian rhythm, Free Radic. Biol. Med. 100 (2016) 73–80.

[24] I.S. Kil, K.W. Ryu, S.K. Lee, J.Y. Kim, S.Y. Chu, J.H. Kim, S. Park, S.G. Rhee, Circadian oscillation of sulfiredoxin in the mitochondria, Mol. Cell. **59** (2015) 651–663.

[25] K. Yamada, K. Yoshida, Mechanical insights into the regulation of programmed cell death by p53 via mitochondria, Biochim. Biophys. Acta Mol. Cell Res. 1866 (2019) 839–848.

[26] B. Liu, Y. Chen, D.K. St Clair, ROS and p53: a versatile partnership, Free Radic. Biol. Med. 44 (2008) 1529–1535.

[27] A.V. Vaseva, N.D. Marchenko, K. Ji, S.E. Tsirka, S. Holzmann, U.M. Moll, P53 opens the mitochondrial permeability transition pore to trigger necrosis, Cell **149** (2012) 1536–1548.

[28] J. Wu, T. Mulatibieke, J. Ni, X. Han, B. Li, Y. Zeng, R. Wan, X. Wang, G. Hu, Dichotomy between receptor-interacting protein 1- and receptor-interacting protein 3-mediated necroptosis in experimental pancreatitis, Am. J. Pathol. 187 (2017) 1035–1048.

[29] X. Ma, D.J. Conklin, F. Li, Z. Dai, X. Hua, Y. Li, Z.Y. Xu-Monette, K.H. Young, W. Xiong, M. Wysoczynski, S.D. Sithu, S. Srivastava, A. Bhatnagar, Y. Li, The oncogenic microRNA miR-21 promotes regulated necrosis in mice, Nat. Commun. 6 (2015) 7151.

[30] Q. Zhao, X. Yu, H. Zhang, Y. Liu, X. Zhang, X. Wu, Q. Xie, M. Li, H. Ying, H. Zhang, RIPK3 mediates necroptosis during embryonic development and postnatal inflammation in fadd-deficient mice, Cell Rep. 19 (2017) 798–808.

[31] A.G. Planson, G. Palais, K. Abbas, M. Gerard, L. Couvelard, A. Delaunay, S. Baulande, J.C. Drapier, M.B. Toledano, Sulfiredoxin protects mice from lipopolysaccharide-induced endotoxic shock, Antioxidants Redox Signal. 14 (2011) 2071–2080.

[32] M.S. Nanadikar, A.M. Vergel Leon, S. Borowik, A. Hillemann, A. Zieseniss, V. V. Belousov, I. Bogeski, P. Rehling, J. Dudek, D.M.O. Katschinski, (2) affects mitochondrial functionality ex vivo, Redox Biol. 22 (2019), 101152.

[33] J.L. Van Laethem, R. Eskinazi, H. Louis, F. Rickaert, P. Robberecht, J. Deviere, Multisystemic production of interleukin 10 limits the severity of acute pancreatitis in mice, Gut 43 (1998) 408–413.

[34] A. Kaczmarek, P. Vandenabeele, D.V. Krysko, Necroptosis: the release of damage-associated molecular patterns and its physiological relevance, Immunity 38 (2013) 209–223.

[35] A. Majdi, L. Aoudjehane, V. Ratziu, T. Islam, M.B. Afonso, F. Conti, T. Mestiri, M. Lagouge, F. Foufelle, F. Ballenghien, T. Ledent, M. Moldes, A. Cadoret, L. Fouassier, J.L. Delaunay, T. Aït-Slimane, G. Courtois, B. Fève, O. Scatton, C. Prip-Buus, C.M.P. Rodrigues, C. Housset, J. Gautheron, Inhibition of receptor-interacting protein kinase 1 improves experimental non-alcoholic fatty liver disease, J. Hepatol. 72 (2020) 627–635.

[36] S. Perez, S. Rius-Perez, I. Finamor, P. Marti-Andres, I. Prieto, R. Garcia, M. Monsalve, J. Sastre, Obesity causes PGC-1alpha deficiency in the pancreas leading to marked IL-6 upregulation via NF-kappaB in acute pancreatitis, J. Pathol. 247 (2019) 48–59.

[37] X. Guo, H. Sesaki, X. Qi, Drp1 stabilizes p53 on the mitochondria to trigger necrosis under oxidative stress conditions in vitro and in vivo, Biochem. J. 461 (2014) 137–146.

[38] F. Napoletano, B. Gibert, K. Yacobi-Sharon, S. Vincent, C. Favrot, P. Mehlen, V. Girard, M. Teil, G. Chatelain, L. Walter, E. Arama, B. Mollereau, P53-dependent programmed necrosis controls germ cell homeostasis during spermatogenesis, PLoS Genet. 13 (2017), e1007024.

[39] L. Pei, Y. Shang, H. Jin, S. Wang, N. Wei, H. Yan, Y. Wu, C. Yao, X. Wang, L.Q. Zhu, Y. Lu, DAPK1-p53 interaction converges necrotic and apoptotic pathways of ischemic neuronal death, J. Neurosci. 34 (2014) 6546–6556.

[40] N.D. Marchenko, S. Wolff, S. Erster, K. Becker, U.M. Moll, Monoubiquitylation promotes mitochondrial p53 translocation, EMBO J. 26 (2007) 923–934.

[41] Y. Zhao, L. Chaiswing, J.M. Velez, I. Batinic-Haberle, N.H. Colburn, T.D. Oberley, D.K. St Clair, P53 translocation to mitochondria precedes its nuclear translocation and targets mitochondrial oxidative defense protein-manganese superoxide dismutase, Cancer Res. 65 (2005) 3745–3750.

[42] A.V. Vaseva, U.M. Moll, The mitochondrial p53 pathway, Biochim. Biophys. Acta **1787** (2009) 414–420.

[43] K. Wang, F. Liu, C.Y. Liu, T. An, J. Zhang, L.Y. Zhou, M. Wang, Y.H. Dong, N. Li, J. N. Gao, Y.F. Zhao, P.F. Li, The long noncoding RNA NRF regulates programmed necrosis and myocardial injury during ischemia and reperfusion by targeting miR-873, Cell Death Differ. 23 (2016) 1394–1405.

[44] I.S. Kil, S.K. Lee, K.W. Ryu, H.A. Woo, M.C. Hu, S.H. Bae, S.G. Rhee, Feedback control of adrenal steroidogenesis via H2O2-dependent, reversible inactivation of peroxiredoxin III in mitochondria, Mol. Cell. **46** (2012) 584–594.

[45] Z. Yang, Y. Wang, Y. Zhang, X. He, C.Q. Zhong, H. Ni, X. Chen, Y. Liang, J. Wu, S. Zhao, D. Zhou, J. Han, RIP3 targets pyruvate dehydrogenase complex to increase aerobic respiration in TNF-induced necroptosis, Nat. Cell Biol. 20 (2018) 186–197.

[46] C. Villeneuve, C. Guilbeau-Frugier, P. Sicard, O. Lairez, C. Ordener, T. Duparc, D. De Paulis, B. Couderc, O. Spreux-Varoquaux, F. Tortosa, A. Garnier, C. Knauf, P. Valet, E. Borchi, C. Nediani, A. Gharib, M. Ovize, M.B. Delisle, A. Parini, J. Mialet-Perez, p53-PGC-1alpha pathway mediates oxidative mitochondrial damage and cardiomyocyte necrosis induced by monoamine oxidase-A upregulation: role in chronic left ventricular dysfunction in mice, Antioxidants Redox Signal. 18 (2013) 5–18.

[47] D. Karunakaran, A.W. Turner, A.C. Duchez, S. Soubeyrand, A. Rasheed, D. Smyth, D.P. Cook, M. Nikpay, J.W. Kandiah, C. Pan, M. Geoffrion, R. Lee, L. Boytard, H. Wyatt, M.A. Nguyen, P. Lau, M. Laakso, B. Ramkhelawon, M. Alvarez, K. H. Pietiläinen, P. Pajukanta, B.C. Vanderhyden, P. Liu, S.B. Berger, P.J. Gough, J. Bertin, M.E. Harper, A.J. Lusis, R. McPherson, K.J. Rayner, RIPK1 gene variants associate with obesity in humans and can be therapeutically silenced to reduce obesity in mice, Nat. Metab 2 (2020) 1113–1125.

[48] J. Gautheron, M. Vucur, A.T. Schneider, I. Severi, C. Roderburg, S. Roy, M. Bartneck, P. Schrammen, M.B. Diaz, J. Ehling, F. Gremse, F. Heymann, C. Koppe, T. Lammers, F. Kiessling, N. Van Best, O. Pabst, G. Courtois, A. Linkermann, S. Krautwald, U.P. Neumann, F. Tacke, C. Trautwein, D.R. Green, T. Longerich, N. Frey, M. Luedde, M. Bluher, S. Herzig, M. Heikenwalder, T. Luedde, The necroptosis-inducing kinase RIPK3 dampens adipose tissue inflammation and glucose intolerance, Nat. Commun. 7 (2016), 11869.

[49] T. Minamino, M. Orimo, I. Shimizu, T. Kunieda, M. Yokoyama, T. Ito, A. Nojima, A. Nabetani, Y. Oike, H. Matsubara, F. Ishikawa, I. Komuro, A crucial role for adipose tissue p53 in the regulation of insulin resistance, Nat. Med. 15 (2009) 1082–1087.

[50] I. Shimizu, Y. Yoshida, T. Katsuno, K. Tateno, S. Okada, J. Moriya, M. Yokoyama, A. Nojima, T. Ito, R. Zechner, I. Komuro, Y. Kobayashi, T. Minamino, P53-induced adipose tissue inflammation is critically involved in the development of insulin resistance in heart failure, Cell Metabol. 15 (2012) 51–64.